Notch induces transcription by stimulating release of paused RNA polymerase II

Julia M. Rogers,[1] Claudia A. Mimoso,[1] Benjamin J.E. Martin,[1] Alexandre P. Martin,[1] Jon C. Aster,[2,3] Karen Adelman,[1,3,4] and Stephen C. Blacklow[1,4,5]

[1]Department of Biological Chemistry and Molecular Pharmacology, Blavatnik Institute, Harvard Medical School, Boston, Massachusetts 02115, USA; [2]Department of Pathology, Brigham and Women's Hospital, Boston, Massachusetts 02215, USA; [3]Ludwig Center at Harvard, Boston, Massachusetts 02115, USA; [4]The Eli and Edythe L. Broad Institute, Cambridge, Massachusetts 02142, USA; [5]Department of Cancer Biology, Dana Farber Cancer Institute, Boston, Massachusetts 02215, USA

Notch proteins undergo ligand-induced proteolysis to release a nuclear effector that influences a wide range of cellular processes by regulating transcription. Despite years of study, however, how Notch induces the transcription of its target genes remains unclear. Here, we comprehensively examine the response to human Notch1 across a time course of activation using high-resolution genomic assays of chromatin accessibility and nascent RNA production. Our data reveal that Notch induces target gene transcription primarily by releasing paused RNA polymerase II (RNAPII). Moreover, in contrast to prevailing models suggesting that Notch acts by promoting chromatin accessibility, we found that open chromatin was established at Notch-responsive regulatory elements prior to Notch signal induction through SWI/SNF-mediated remodeling. Together, these studies show that the nuclear response to Notch signaling is dictated by the pre-existing chromatin state and RNAPII distribution at the time of signal activation.

[*Keywords*: ATAC-seq; NOTCH1; Notch signaling; PRO-seq; SWI/SNF; TT-seq]

Supplemental material is available for this article.

Received July 12, 2024; revised version accepted September 24, 2024.

Cells reliably and precisely convert signaling inputs into cellular decisions by inducing gene expression programs that specify cellular identity. Notch–Delta signaling is one of several essential metazoan pathways of cell–cell communication that guides cell fate decisions in organismal development and homeostasis across tissues and organ systems (Siebel and Lendahl 2017). Notch signaling is dysregulated in multiple cancer types, including T-cell acute lymphoblastic leukemia, which is associated with gain-of-function mutations in *NOTCH1*, and squamous cell carcinoma, which is associated with loss of function of *NOTCH1, NOTCH2*, and/or *NOTCH3* (Aster et al. 2017).

Notch proteins, the receiver components of this signaling system, are single-pass transmembrane receptors that have an extracellular ligand-binding domain, a juxtamembrane regulatory domain, and an intracellular effector domain (NICD) that is liberated by ligand-induced proteolysis to function as a transcriptional effector (Bray and Gomez-Lamarca 2018). In the nucleus, NICD forms a multiprotein Notch transcriptional complex (NTC) with a DNA-binding transcription factor called RBPJ in mammals (*suppressor of hairless* in flies) and a protein of the Mastermind-like (MAML) family. Formation of the NTC leads to transcription of target genes.

Notch signals activate a vastly different array of transcriptional targets in each cell type, allowing this key regulator to have distinct cellular effects depending on the cellular context (Bray and Gomez-Lamarca 2018). As a result, Notch signaling can be oncogenic or tumor-suppressive depending on the cancer type (Aster et al. 2017). However, how the cell type specificity of Notch targets is achieved and how the NTC stimulates transcription remain unclear at the molecular level. Understanding the molecular mechanisms by which Notch signaling induces transcription is key to understanding how this essential signaling pathway functions in development and disease.

Transcription factors (TFs) can stimulate RNA polymerase II (RNAPII)-dependent transcription at multiple steps in the transcription cycle, including during the establishment of chromatin accessibility, RNAPII recruitment to promoters and transcription initiation, or the release of paused RNAPII into productive elongation (Adelman and Lis 2012; Core and Adelman 2019). Previous work has led to conflicting models of how the NTC

Corresponding authors: stephen_blacklow@hms.harvard.edu, karen_adelman@hms.harvard.edu
Article published online ahead of print. Article and publication date are online at http://www.genesdev.org/cgi/doi/10.1101/gad.352108.124.

stimulates transcription. The prevailing model suggests that the NTC cooperates with chromatin remodelers to increase chromatin accessibility (Pillidge and Bray 2019). Consistent with this idea, genetic associations between components of the SWI/SNF chromatin remodeler complex and Notch signaling have been observed in both mice and flies (Takeuchi et al. 2007; Pillidge and Bray 2019). Immunoprecipitation followed by mass spectrometry, coimmunoprecipitation, and proximity labeling studies have also suggested that components of the SWI/SNF complex may associate with or are in the molecular neighborhood of Notch1 (Kadam and Emerson 2003; Takeuchi et al. 2007; Yatim et al. 2012; Martin et al. 2023a). Notably, cells maintained in a persistent Notch-on state have higher chromatin accessibility at Notch binding sites than cells in a Notch-off state (Gomez-Lamarca et al. 2018; Pillidge and Bray 2019). Moreover, knockdown of SWI/SNF components in cells in a persistent Notch-on state reduces chromatin accessibility and reduces transcription of Notch-responsive genes (Yatim et al. 2012; Pillidge and Bray 2019).

Other observations are less consistent with a model in which Notch directly interacts with or recruits SWI/SNF to promote chromatin accessibility. For example, BRM (SMARCA2), a catalytic subunit of the SWI/SNF complex, was shown to be present at some Notch-responsive promoters prior to Notch activation in mouse cells (Kadam and Emerson 2003). Indeed, chromatin compaction can restrict Notch activity, and NTC binding is limited to regions of already accessible chromatin with epigenetic signatures associated with active regulatory regions (Skalska et al. 2015; van den Ameele et al. 2022). These findings suggest an alternative model in which gene activation upon Notch signaling relies on cell type-specific transcription factors that establish the proper chromatin context for Notch activation in different cellular contexts (Wang et al. 2011; Skalska et al. 2015; Falo-Sanjuan et al. 2019). The fact that Notch signaling induces different programs of gene expression in different cell types (Aster 2020) is also consistent with a model in which the NTC acts on pre-existing, poised regulatory regions.

Whether and how the interplay between NTC and chromatin remodeling complexes drives specific gene expression upon Notch activation remain poorly understood, largely because studies investigating the dynamics of NTC recruitment and gene activation lack the temporal resolution needed to distinguish direct effects from indirect effects. We thus sought to elucidate, with high temporal and genomic resolution, how Notch activation induces transcription. We monitored the genome-wide response to human Notch1 as a function of time after activation in Notch-naïve squamous cell carcinoma (SCC) cells. Newly synthesized RNAs were measured using transient transcriptome sequencing (TT-seq), accessibility was monitored by the assay for transposase-accessible chromatin with sequencing (ATAC-seq), and active RNAPII was mapped using precision run-on sequencing (PRO-seq). Strikingly, we found that the chromatin accessibility of NTC binding sites did not increase in response to Notch activation. Instead, we found that SWI/SNF establishes accessibility at Notch-responsive regulatory elements prior to signaling, allowing Notch to rapidly bind these loci upon activation. Importantly, we defined the step in the transcription cycle regulated by Notch, finding that the NTC predominantly acts by releasing paused RNAPII into productive elongation at target genes. Together, our data elucidate how cellular context and the pre-existing chromatin landscape dictate the specificity of the Notch transcriptional response, providing a conceptual and experimental framework for a better understanding of signal-responsive gene expression.

Results

Cellular system for time-resolved studies

To study how Notch induces transcription, we used the SC2 squamous cell carcinoma cell line (Pan et al. 2020), which is engineered to express a ligand-independent, autonomously active form of human Notch1 (ΔEGF-L1596H) that can be silenced by γ-secretase inhibitor (GSI) treatment. SC2 cells can be maintained in a Notch-naïve state by culturing cells in the presence of GSI. When GSI is washed out, SC2 cells rapidly transition from a Notch-off to a Notch-on state, thereby enabling the measurement of the direct response of these cells to Notch activation (Pan et al. 2020). These features provide distinct advantages for kinetic assessment of how cell state and chromatin context affect the genomic response to a Notch signal.

Identification of Notch target genes

We identified direct Notch target genes in SC2 cells by performing TT-seq at 1 and 4 h time points after inducing Notch activity by GSI washout (Fig. 1A). TT-seq is a metabolic labeling approach used to identify and quantify newly synthesized RNAs (Schwalb et al. 2016) and therefore enabled us to define genes induced at specific times after Notch activation. These early time points after Notch activation were chosen to enrich for direct transcriptional responses to Notch activity. To identify specific Notch targets, we included matched time point mock washout control samples, which were subjected to the same manipulations and media change as the GSI washout samples, but GSI was maintained in the media. Notably, most of the genes induced in response to GSI washout were also induced in the mock washout (Fig. 1B; Supplemental Fig. S1A), indicating a strong general impact of these cellular manipulations and highlighting the importance of this experimental control.

We classified gene responses into four categories to separate Notch-dependent transcriptional responses from Notch-independent ones: Notch-upregulated (upregulated in GSI washout but not mock washout; $n = 61$), Notch-downregulated (downregulated in GSI washout but not mock washout; $n = 93$), nonspecific upregulated (upregulated in both GSI and mock washout; $n = 997$), and nonspecific downregulated (downregulated in both

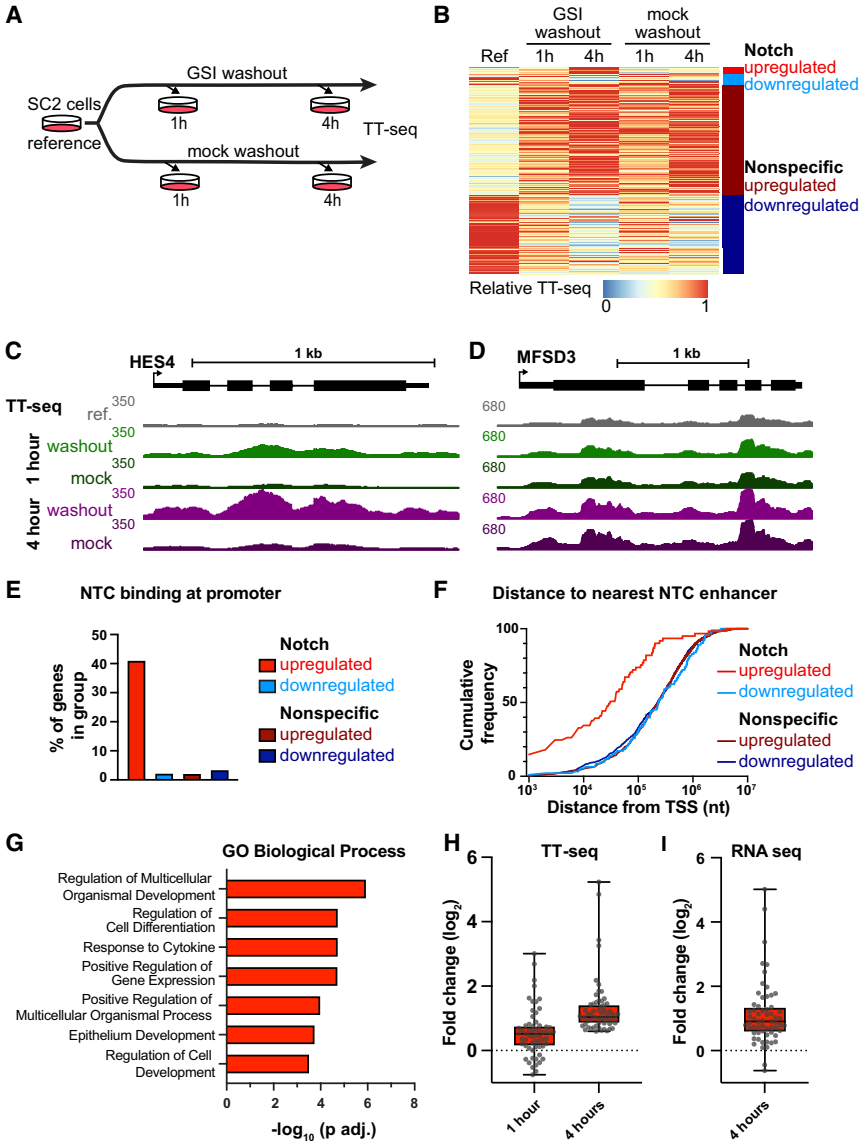

Figure 1. Identification of high-confidence Notch target genes in SCC cells. (*A*) Design of the TT-seq experiment. The reference sample was subjected to mock washout, immediately incubated with labeling media for 10 min, and then harvested. The 1 and 4 h samples were subjected to mock or GSI washout and incubated with labeling media for the 10 min preceding harvest at the indicated times. (*B*) Heat map indicating relative TT-seq signal over exons for significantly changed genes. Color bars at the *right* indicate gene groups. (Red) Notch-upregulated ($n = 61$), (light blue) Notch-downregulated ($n = 93$), (dark red) nonspecific upregulated ($n = 997$), (dark blue) nonspecific downregulated ($n = 711$). (*C*,*D*) Genome browser images showing sense strand TT-seq reads for a representative Notch-upregulated gene (*HES4*; *C*) and a representative nonspecific upregulated gene (*MFSD3*; *D*). (*E*) The percentage of genes with Notch transcription complex (NTC) binding (Pan et al. 2020) at the promoter plotted for each gene group. (*F*) Cumulative distribution plot of the distance from the TSS of genes in each group to the nearest NTC-bound enhancer. (*G*) Top gene ontology biological process-enriched terms for genes in the Notch-upregulated group. *P*-values are from the hypergeometric test, corrected for multiple hypotheses according to the Benjamini–Hochberg method. (*H*) Box plots showing the fold change ($\log_2$) in TT-seq exon counts for Notch-upregulated genes at 1 and 4 h, compared with the reference condition. The *middle* line indicates the median, the box represents the 25th and 75th percentile, and whiskers show the largest or smallest value in the data set. (*I*) Box plots (rendered as in *H*) showing the fold change ($\log_2$) in RNA-seq gene counts for Notch-upregulated genes relative to the mock washout condition at 4 h. RNA-seq data are from Pan et al. (2020). See also Supplemental Figure S1.

GSI and mock washout; $n = 711$) (Supplemental Table S1). As anticipated, the Notch-upregulated gene *HES4* was specifically induced under GSI washout but not mock washout conditions (Fig. 1C), whereas a representative nonspecific upregulated gene (*MFSD3*) was activated in both conditions (Fig. 1D).

To further validate that the Notch-upregulated genes are direct targets of Notch activity, we analyzed genomic binding by Notch transcription complex (NTC) components in SC2 cells (Pan et al. 2020). For this analysis, we defined NTC binding sites as those loci exhibiting both RBPJ and MAML1 binding by ChIP-seq 4 h after GSI washout. We found that Notch-upregulated genes are much more likely to have NTC binding sites within 1 kb of their transcription start sites, and that these genes are much closer to NTC-bound enhancers than genes within the three other groups (Fig. 1E,F), consistent with enrichment within this group of genes for direct regulation in response to NTC binding. In contrast, the lack of NTC binding near genes that are downregulated upon GSI washout suggests that gene repression in response to Notch activation is not mediated directly by NTC binding. This repression may instead result from secondary effects, such as Notch induction of transcriptional repressors like the HES genes. The Notch-upregulated gene set contained canonical Notch targets upregulated in many cell types (*HES1*, *HES4*, and *NRARP*), known Notch targets in squamous cells (*IER5* and *RHOV*), and targets not previously associated with Notch signaling (*CELSR2* and *ADGRG6*). The biological process GO terms for this group of genes included terms associated with development and differentiation, consistent with the role of Notch signaling in determining cell fate (Fig. 1G). In contrast, the genes whose expression changed in response to mock washout are enriched for GO terms associated with metabolism and biosynthesis, consistent with a response to the

replenishment of nutrients in the fresh media used during washout (Supplemental Fig. S1B–D).

Although some Notch-upregulated genes are induced within 1 h of GSI washout, they showed maximal expression at 4 h after GSI washout (Fig. 1H). Consistent with the increase in RNA synthesis observed in TT-seq, these genes were also induced in published steady-state RNA-seq performed in these cells following 4 h of GSI washout (Fig. 1I; Pan et al. 2020).

Notch activates gene expression without increasing chromatin accessibility

Prior studies have found that Notch binding sites in "Notch-on" cells have higher chromatin accessibility at steady state than in "Notch-off" cells (Gomez-Lamarca et al. 2018; Pillidge and Bray 2019). We therefore tested whether Notch directly affects the chromatin landscape by monitoring dynamic changes in chromatin accessibility at time points up to 4 h after Notch induction by GSI washout using ATAC-seq (Fig. 2A; Supplemental Fig. S2A; Buenrostro et al. 2013; Grandi et al. 2022). Notch-upregulated genes have accessible promoters prior to Notch induction, based on the significant levels of promoter-proximal ATAC-seq reads observed in the reference condition (Fig. 2B). This observation highlights how the basal context of a cell, likely defined by other transcription factors, can determine where the NTC can induce gene activity and is consistent with prior literature showing that Notch activity requires a permissive chromatin environment (Wang et al. 2011; Skalska et al. 2015; Falo-Sanjuan et al. 2019; van den Ameele et al. 2022).

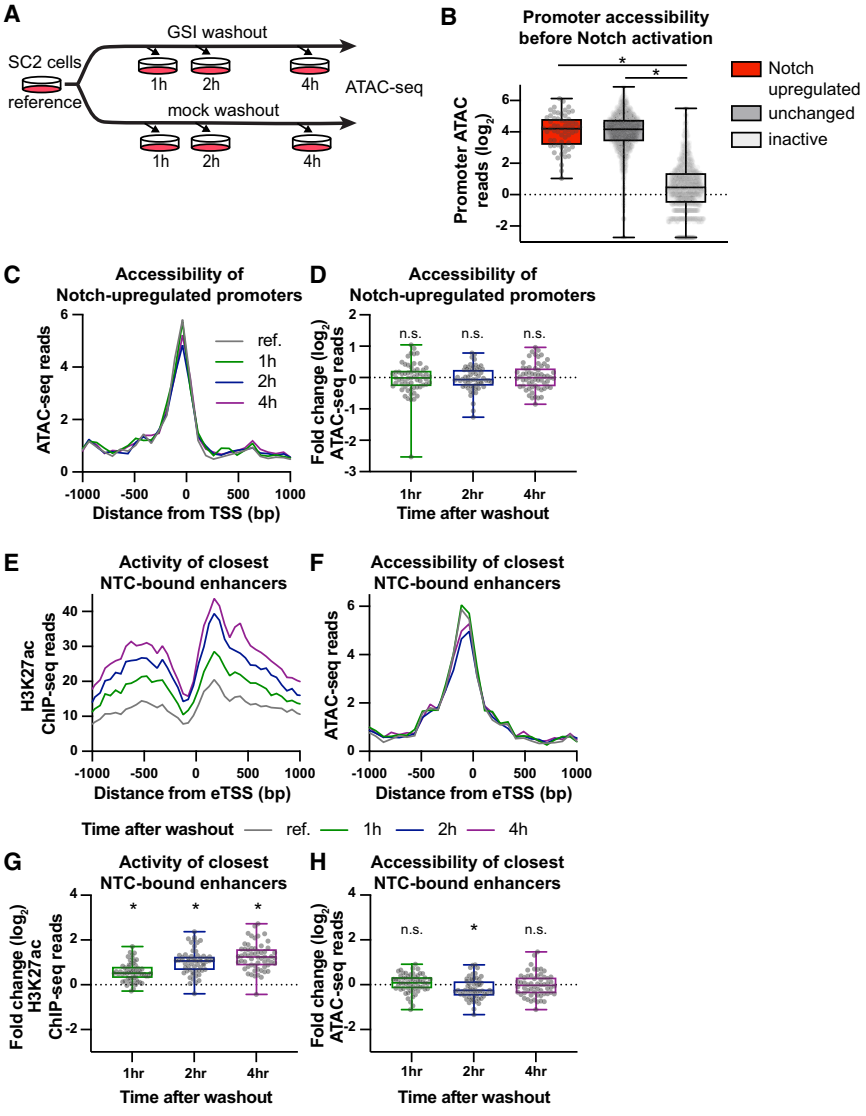

Figure 2. Notch activation does not increase chromatin accessibility. (*A*) Design of the ATAC-seq experiment. The reference condition was subjected to mock washout and then immediately harvested. All other samples were harvested at the indicated times after GSI washout. (*B*) Box plots (rendered as in Fig. 1H) showing ATAC-seq reads ($\log_2$) over the promoters (TSS − 450 to TSS + 149) of Notch-upregulated genes ($n = 61$), unchanged genes ($n = 51{,}484$), and inactive genes ($n = 1295$) prior to Notch activation. Unchanged genes are defined as genes with a TT-seq gene body read $|FC| < 1.1$ in the 1 h washout and 4 h washout conditions compared with the reference. Lowly active genes (inactive) are defined as genes with <10 PRO-seq reads within the promoter region (TSS to TSS + 150) at any time point. Asterisks indicate significant differences (P adj. < 0.05) in accessibility by Dunn's multiple comparisons test. (*C*) Aggregate plot showing ATAC-seq reads around promoters of Notch-upregulated genes ($n = 61$). ATAC-seq reads are shown in 75 bp bins. (*D*) Box plots (rendered as in *B*) showing fold change ($\log_2$) in ATAC-seq reads at the promoter (TSS − 450 to TSS + 149) for Notch-upregulated genes ($n = 61$). "n.s." indicates conditions not significantly different (P adj. > 0.05) from a fold change of 0 (Wilcoxon signed rank test; P-values corrected according to the Benjamini–Hochberg method). (*E*,*F*) Aggregate plots showing H3K27ac ChIP-seq (*E*) or ATAC-seq (*F*) reads at the closest NTC-bound enhancers with identified enhancer TSSs (eTSSs) (see the Materials and Methods) to Notch-upregulated genes ($n = 56$). Plots are centered around the eTSSs. *E* is shown in 50 bp bins, and *F* is in 75 bp bins. (*G*,*H*) Box plots (rendered as in *B*) showing fold change ($\log_2$) in H3K27ac ChIP-seq (*G*) or ATAC-seq (*H*) reads at NTC-bound enhancers closest to Notch-upregulated genes ($n = 58$). Asterisks indicate conditions significantly different (P adj. < 0.05) from a fold change of 0 (Wilcoxon signed rank test; P-values corrected according to the Benjamini–Hochberg method). See also Supplemental Figure S2.

We next investigated whether Notch activation affects the accessibility of responsive promoters. Aggregate plots around gene promoters and counting of the total ATAC-seq reads over the promoters of Notch-upregulated genes showed no changes in promoter accessibility over the 4 h time course (Fig. 2C,D) despite clear increases in gene expression. These observations are inconsistent with a model in which Notch recruits SWI/SNF complexes to open up target gene promoters, instead suggesting that NTCs act on loci that are accessible prior to Notch activation.

Because most Notch genomic binding occurs at distal regulatory regions in other cell types (Wang et al. 2014), we also examined whether Notch activation affects the accessibility of Notch-responsive enhancers. We defined NTC-bound regions as those occupied by both NTC subunits RBPJ and MAML1 in published ChIP-seq data (Pan et al. 2020) and used these data to identify the NTC-bound enhancer closest to each Notch-upregulated gene (see the Materials and Methods). We then examined the activity of these enhancers in a 4 h time course after Notch induction by GSI washout. Enhancer activity, as judged by H3K27ac chromatin immunoprecipitation followed by sequencing (ChIP-seq) (Fig. 2E,G), increased over the 4 h time course, confirming that these elements are high-confidence Notch-responsive enhancers. Importantly, control non-NTC-bound enhancers near genes that do not exhibit changes in expression as assessed by TT-seq did not show this increase in H3K27ac ChIP-seq signal following Notch activation (Supplemental Fig. S2B). The NTC-bound enhancers, however, did not show increased accessibility following GSI washout in either aggregate plots or read counts over the enhancers, in agreement with our findings at Notch-responsive promoters (Fig. 2F,H). Together, these findings argue against models in which Notch activation induces gene expression through modulation of chromatin accessibility at either promoters or enhancers. Instead, our data favor a mechanism in which Notch binding occurs at pre-existing open regulatory regions.

SWI/SNF activity is required to maintain promoter accessibility

Although chromatin accessibility was not increased at sites of Notch-dependent gene induction, previous studies have shown strong associations between the SWI/SNF chromatin remodeling complex and Notch activity (Takeuchi et al. 2007; Pillidge and Bray 2019). To elucidate the basis for the interplay between SWI/SNF and Notch, we performed TT-seq to examine newly synthesized transcripts at 1 and 4 h time points after Notch activation in the presence of an allosteric inhibitor of SWI/SNF activity (Supplemental Fig. S3A), BRM014, which rapidly inactivates the SWI/SNF ATPase, resulting in decreased promoter and enhancer accessibility (Papillon et al. 2018; Iurlaro et al. 2021; Schick et al. 2021; Martin et al. 2023b). Adding BRM014 at the time of Notch activation blocked the induction of 41 of the 61 Notch-upregulated genes (Fig. 3A), consistent with previous work linking SWI/SNF activity to Notch-dependent gene activation. Chromatin accessibility in the reference condition was not different between SWI/

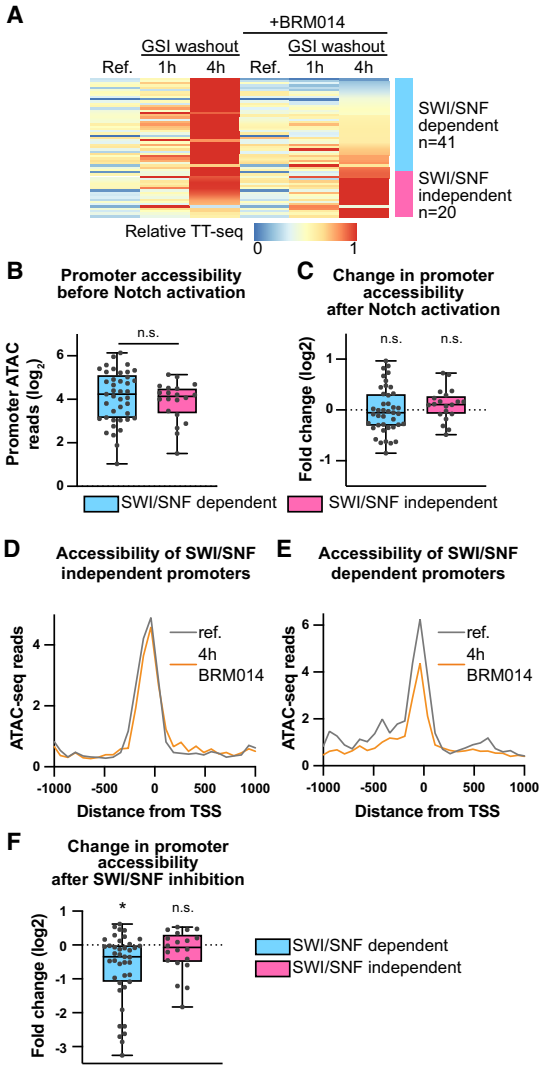

Figure 3. SWI/SNF activity is required to keep most promoters accessible for activated Notch. (*A*) Heat map indicating relative TT-seq signal over exons for Notch-upregulated genes. Color bars at the *right* indicate gene groups. (Blue) SWI/SNF-dependent ($n = 41$), (pink) SWI/SNF-independent ($n = 20$). (*B*) Box plots (rendered as in Fig. 1H) showing ATAC-seq reads ($\log_2$) over the promoters (TSS − 450 to TSS + 149) of SWI/SNF-dependent and SWI/SNF-independent genes. "n.s." indicates groups not significantly different ($P > 0.05$) by Mann–Whitney test. (*C*) Box plots (rendered as in *B*) showing fold change ($\log_2$) in ATAC-seq reads at the promoter (TSS − 450 to TSS + 149) for SWI/SNF-dependent and SWI/SNF-independent genes at 4 h after Notch activation compared with the reference condition. "n.s." indicates conditions not significantly different ($P > 0.05$) from a fold change of 0 (Wilcoxon signed rank test). (*D*,*E*) Aggregate plot showing ATAC-seq reads around promoters of SWI/SNF-independent (*D*) and SWI/SNF-dependent (*E*) genes. ATAC-seq reads are shown in 75 bp bins. Gray indicates the reference condition (ref.), and orange indicates 4 h of mock washout + BRM014. (*F*) Box plots (rendered as in *B*) showing fold change ($\log_2$) in ATAC-seq reads at the promoter (TSS − 450 to TSS + 149) for SWI/SNF-dependent and SWI/SNF-independent genes at 4 h after mock washout in the presence of BRM014, compared with the reference condition. Asterisks indicate conditions significantly different ($P < 0.05$) from a fold change of 0 (Wilcoxon signed rank test). See also Supplemental Figure S3.

SNF-dependent or SWI/SNF-independent gene groups (Fig. 3B), and neither subgroup showed any change in chromatin accessibility after Notch induction (Fig. 3C). We also performed ATAC-seq at 1, 2, and 4 h time points after Notch activation in the presence of BRM014 (Supplemental Fig. S3B) and found that, as expected, SWI/SNF-independent genes did not exhibit a significant change in accessibility following BRM014 treatment (Fig. 3D,F). However, adding BRM014 at the time of mock (Fig. 3E,F) or GSI (Supplemental Fig. S3C–E) washout revealed a rapid and significant decrease in ATAC-seq signal at SWI/SNF-dependent promoters. Importantly, because loss of accessibility upon BRM014 treatment was observed under both mock and GSI washout conditions, the sensitivity of promoter accessibility to SWI/SNF appears to be independent of the Notch activation status of the cells. These data suggest that SWI/SNF-dependent promoters require persistent SWI/SNF activity to remain accessible, independent of whether Notch is active. Suppression of SWI/SNF activity, even at the time of GSI washout, is sufficient to reduce chromatin accessibility and prevent Notch-mediated gene activation.

Notch-upregulated genes are activated by release of paused RNAPII

If Notch is not acting to increase chromatin accessibility, how does it stimulate transcription? To address this question, we performed PRO-seq (Kwak et al. 2013; Mahat et al. 2016) to measure the effect of activated Notch on RNAPII at a series of time points from 15 min up to 4 h after GSI washout (Fig. 4A; Supplemental Fig. S4A). PRO-seq maps the location of engaged RNAPII across the genome, which allowed us to measure both gene body transcription and RNAPII occupancy at promoters. Notch-

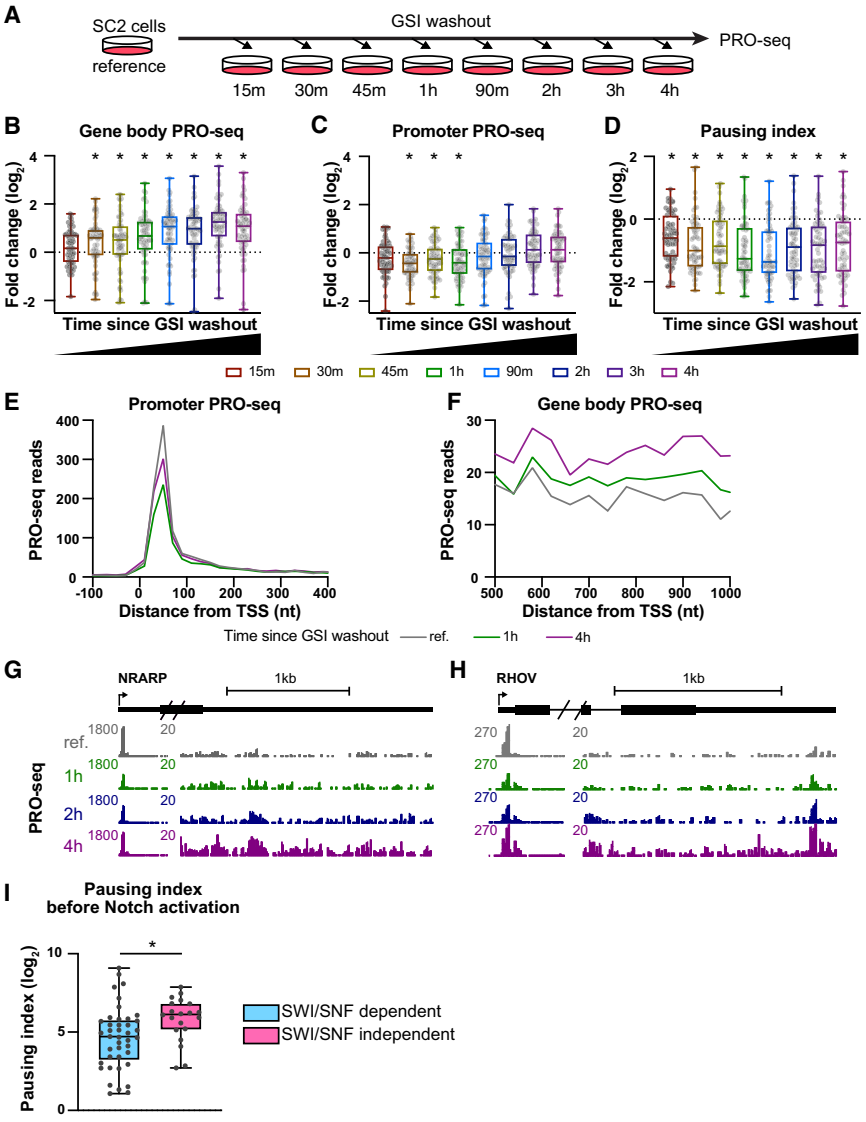

Figure 4. Notch-dependent genes are activated by pause release. (*A*) Design of the PRO-seq experiment. The reference condition was subjected to mock washout and then immediately harvested. All other samples were harvested at the indicated times after GSI washout. (*B*,*C*) Box plots (rendered as in Fig. 1H) showing the fold change ($\log_2$) in PRO-seq gene body (*B*) or promoter (*C*) counts for Notch-upregulated genes compared with the reference condition. Gene body windows are defined as TSS + 250 bp to TSS + 5 kb, and promoter windows are defined as TSS to TSS + 150 bp. Asterisks indicate conditions significantly different (P adj. < 0.05) from a fold change of 0 (Wilcoxon signed rank test; P-values corrected according to the Benjamini–Hochberg method). (*D*) Box plots (rendered as in Fig. 1H) showing the fold change ($\log_2$) in pausing index compared with the reference condition for Notch-upregulated genes. Pausing index is defined as promoter counts per kilobase/gene body counts per kilobase. Asterisks indicate conditions significantly different (P adj. < 0.05) from a fold change of 0 (Wilcoxon signed rank test, P-values corrected according to the Benjamini–Hochberg method). (*E*) Aggregate plots showing average reads of PRO-seq signal around promoters of Notch-upregulated genes. Data are plotted in 20 bp bins. (*F*) Aggregate plots showing average reads of PRO-seq signal in the gene bodies of Notch-upregulated genes. Data are plotted in 40 bp bins. (*G*,*H*) Genome browser images showing PRO-seq reads for Notch-upregulated genes *NRARP* (*G*) and *RHOV* (*H*). The scale of the browser images is reset at 500 bp downstream from the TSS to allow visualization of the gene body signal. (*I*) Box plots (rendered as in *B*) showing pausing index of SWI/SNF-dependent and SWI/SNF-independent genes in the reference condition. Asterisks indicate groups significantly different (P < 0.05) by Mann–Whitney test. See also Supplemental Figure S4.

upregulated genes showed an increase in PRO-seq signal in the gene body within 30 min of Notch activation (Fig. 4B) that persisted over the time course, consistent with direct upregulation of these genes by increased transcription. If Notch activation served to increase the recruitment of RNAPII or transcription initiation, we should have observed an increase in PRO-seq signal at Notch-upregulated promoters over this time window. However, the promoter PRO-seq signal did not increase upon Notch activation and was instead significantly decreased at 30 min and 1 h after GSI washout (Fig. 4C). We conclude that Notch activation does not primarily increase transcription by stimulating initiation.

Transcription can be induced by stimulating transcription initiation or promoting the release of paused RNAPII. To evaluate whether Notch activation impacted pause release, we calculated the pausing index for the Notch-upregulated genes over time. The pausing index, a ratio of promoter to gene body PRO-seq reads, indicates the level of RNAPII pausing for each gene. We found that the pausing index decreased significantly at Notch-upregulated genes as early as 15 min after Notch activation (Fig. 4D), implicating a pause release mechanism in Notch-dependent gene activation. Genes that are nonspecifically upregulated in response to the media change do not show this same sustained reduction in pausing index (Supplemental Fig. S4B), suggesting that this pause release mechanism is specific to the Notch response.

Aggregate plots showing the average signal around promoters and gene bodies of the Notch-upregulated genes further support the presence of a pause release mechanism (Fig. 4E,F). At 1 h after Notch activation, there were fewer PRO-seq reads at the promoter and more in the gene body, indicative of the transition of RNAPII from pausing to productive elongation. By 4 h, the gene body signal increased further, and the promoter signal rebounded to approach that of the reference condition, consistent with reinitiation after the initial release of paused RNAPII.

Browser shots of two Notch-regulated genes, *NRARP* (Fig. 4G) and *RHOV* (Fig. 4H), further highlight the effect of Notch activation in stimulating pause release. In the reference condition (i.e., before Notch activation), both promoters exhibit a peak of paused RNAPII proximal to the promoter with very low signal in the gene body. At 1 h, a decrease in the paused peak is accompanied by release of RNAPII into the gene body, with the highest gene body signal observed at 4 h. There is also restoration of the PRO-seq signal at the promoter at 4 h, consistent with increased transcriptional initiation by RNAPII at this time point. This delayed stimulation of initiation is particularly evident for the canonical Notch-responsive gene HES1, which responds rapidly to Notch activation and shows oscillations in PRO-seq signal over time, with a period of ~2 h, consistent with previous studies (Supplemental Fig. S4C; Hirata et al. 2002).

Because RNAPII pausing has been associated with maintaining promoter accessibility (Gilchrist et al. 2010), we asked whether pausing itself could explain the SWI/SNF independence of some of the Notch-responsive genes. We found that the SWI/SNF-independent genes exhibited a significantly higher pausing index than genes that were sensitive to acute SWI/SNF inhibition (Fig. 4I). Therefore, we propose that there are two mechanisms by which promoters can be maintained in a Notch-responsive state (Fig. 5). For most responsive genes, SWI/SNF is required both to establish chromatin accessibility and to maintain promoters in a Notch-responsive state, allowing direct binding of NTC to either the promoter or enhancer to promote RNAPII pause release. For a smaller proportion of genes, high levels of stably paused RNAPII can maintain promoter accessibility in the absence of SWI/SNF activity, allowing access by NTC upon Notch pathway activation, even when SWI/SNF is inhibited.

Discussion

Using time-resolved genomic approaches in Notch-naïve SC2 cells, we found that activated Notch stimulates gene activity primarily by promoting release of paused RNAPII. Our data also revealed that NTCs activate preexisting accessible sites rather than induce regions of chromatin accessibility. These findings clarify the associations between SWI/SNF and Notch activation, demonstrating the importance of SWI/SNF for establishing, and in most cases maintaining, the permissive chromatin state needed for stable NTC genomic binding and Notch-dependent gene induction. The reliance of NTCs on the prior opening of chromatin by other transcription factors rationalizes why Notch signaling is able to induce expression of different target genes in different cell types and underscores the cooperation of Notch nuclear complexes with distinct TFs in each cell type. Our findings dovetail nicely with other systems in which signal-responsive and developmentally regulated expression programs are coordinated by combinations of TFs, with lineage-determining TFs establishing the genomic landscape of accessible regulatory elements that are available for binding by signal-responsive TFs (Heinz et al. 2010;

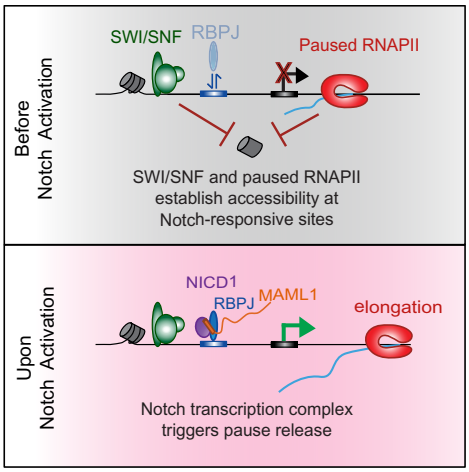

Figure 5. Model figure depicting the pause release mechanism for NTC-induced transcription.

Lefterova et al. 2010; Biddie et al. 2011; Chambers et al. 2023). We speculate that other signal-dependent transcription networks may function similarly, with signal-responsive TFs themselves playing little role in defining chromatin accessibility. Instead, chromatin remodelers can collaborate with other TFs (e.g., PU.1) (Heinz et al. 2010; Chambers et al. 2023) prior to signal induction to generate the appropriate chromatin landscape for cell type- or condition-specific binding of signal-responsive TFs. Indeed, like the NTC, NF-κB also binds to previously accessible chromatin (Utley et al. 1997; Saccani et al. 2001; Weinmann et al. 2001) and has been implicated in regulating transcription elongation and pause release (Adelman et al. 2009; Hargreaves et al. 2009), highlighting parallels between Notch signaling and inflammatory pathways.

Although we have shown here that the NTC does not need to open chromatin to activate transcription, other groups have shown that accessibility is higher at Notch-responsive elements in cases of sustained Notch signaling (Pillidge and Bray 2019), which could be due to the NTC itself or other secondary factors induced by Notch. These longer-term changes in chromatin accessibility are likely to be important for opening and activating new regulatory elements in developmental or disease contexts where Notch signaling triggers changes in cellular state. It is also well established that Notch activation results in increased RBPJ [or Su(H)] ChIP signal at responsive binding sites (Krejčí and Bray 2007; Castel et al. 2013; Wang et al. 2014). The increased RBPJ signal, however, need not require changes in accessibility at these sites but could instead result from an increase in stability of the DNA-bound state of RBPJ in the context of the NTC and/or other recruited transcriptional coactivators. These studies, performed in asynchronous cells, also do not address the potential for interplay among Notch signaling, chromatin accessibility, and the cell cycle, which have very different temporal dynamics.

Several features of our experimental design—synchronization of Notch activation by GSI washout, time-resolved analyses of gene induction, readouts of nascent transcription, and rapid-acting SWI/SNF inhibitors—made it possible to observe direct responses to Notch signal activation and draw mechanistic inferences from these studies. Notably, the rigorous setup of our system allowed us to observe a substantial effect of media change, apparent in our mock washout matched time point controls. This finding raises a concern that should be taken into account by the gene expression field anytime that media washout or exchange is used to identify transcriptional targets (e.g., when GSI washout is used to identify Notch-induced genes). Accordingly, by rigorously filtering out nonspecific effects, we identified fewer Notch target genes than described in some studies but found the genes identified to be high-confidence, direct targets. Indeed, the number of Notch-regulated genes studied here is comparable with that seen in studies identifying Notch targets in T-cell acute lymphoblastic leukemia/lymphoma (Weng et al. 2006).

Why might a pause release mechanism be advantageous for the action of Notch nuclear complexes? RNAPII pausing is known to promote synchronicity in gene activation; for example, in the context of developing fly embryos to ensure coordinated cell behavior in tissue development (Boettiger and Levine 2009; Lagha et al. 2013). Because Notch signals act at discrete times during tissue development to direct cell fate decisions, the stimulation of RNAPII pause release by Notch can direct precise timing of responses and specify robustness in cell fate choices in response to a Notch signal. Given these considerations, one developmental process that appears well suited to a pause release mechanism of gene regulation is somitogenesis, where Notch signals in the segmentation clock are highly synchronous. Interestingly, canonical Notch target genes, including *HES1*, *HES2*, and *HES4*, fall into the SWI/SNF-independent gene group with higher levels of paused RNAPII, consistent with these core targets being primed for robust and synchronous Notch responsiveness.

In conclusion, our data support a new pause release model for Notch-mediated gene activation. This model establishes the groundwork for future inquiry into the identity of transcription factors responsible for establishing the landscape of paused RNAPII that Notch can act on in distinct cell types, as well as the basis of how NTC binding promotes RNAPII release. p300 activity is stimulated at NTC targets in response to Notch activation, and the interaction between the MAML1 subunit of the NTC and p300 is required for Notch-dependent gene activation (Fryer et al. 2002; Saint Just Ribeiro et al. 2007; Rogers et al. 2020). This dependence suggests that pause release may be stimulated by histone acetylation, coupled to binding of BRD4 to acetylated histone tails and the stimulation of P-TEFb activity at Notch-responsive promoters (Core and Adelman 2019). Additionally, it has been reported that the NTC can interact with components of the superelongation complex (SEC) in flies and could potentially directly recruit P-TEFb to its target genes (Liu et al. 2017). It will be interesting in future work to identify the mechanism by which Notch promotes pause release and to determine whether these partners of Notch are conserved or distinct across various tissues and Notch-associated cancers.

Materials and methods

Cell culture and washout protocol

SC2 squamous cell carcinoma cells (Pan et al. 2020) were cultured in keratinocyte media (see the Supplemental Material). γ-Secretase inhibitor (GSI) was prepared as a 1 mM stock of compound E (EMD Millipore 565790) in DMSO (Sigma-Aldrich 472301). Cells were split every 3–4 days using 0.25% trypsin (VWR 45000-664) supplemented with 1 μM GSI. Cells were incubated in 0.25% trypsin at 37°C until cells began to slough off the plate and then were quenched with fresh media and replated. Cells were routinely tested for mycoplasma and used for experiments within 1 month of thawing a fresh vial.

For all GSI washouts, media was removed, and cells were washed twice with media containing 0.1% DMSO

instead of GSI and replenished with media containing 0.1% DMSO instead of GSI, for a total of three media changes. In the mock washouts, both the washing media and the replenishing media contained 1 μM GSI. For experiments with BRM014 (MedChem Express HY-119374), the replenishing media, but not the washout media, contained either 1 μM BRM014 or 0.01% DMSO depending on the sample.

TT-seq sample preparation and library construction

The evening before the time course, eleven 15 cm dishes were seeded with 10 million SC2 cells per plate in SC2 media with 1 μM GSI. Ten plates were used for sample conditions, and the 11th plate was used as a sentinel plate. Cells were harvested from this plate using 0.25% trypsin and were counted to determine the total number of cells per plate. For each replicate, it was assumed that all 10 experimental plates had the same number of cells as the sentinel plate. Replicates were performed on different days ($n = 2$).

Washouts and mock washouts were performed as described above in the GSI washout section. BRM014 (1 μM) or the equivalent volume of DMSO was added in the replenishing media after the two media changes. Labeling was performed for 10 min in 15 mL of media supplemented with 500 μM 4-thiouridine (4-SU) (Thermo Fisher J60679) with GSI and/or BRM014 depending on the experimental condition. For the 0 h time points, labeling media was added immediately after the mock washouts. For the 1 h and 4 h time points, labeling media was added at 50 min or 3 h and 50 min after washout, respectively. To harvest cells for TT-seq, plates were quickly rinsed with 20 mL of PBS, and then 2 mL of Trizol (Thermo Scientific 15596026) was added to the plate. After 3 min of lysis in the dish, the cell lysate in Trizol was collected and frozen at −80°C. To prepare RNA, 1.4 mL of each sample was used. For normalization purposes, fly spike-in cells were used. RNA was then purified and used as input for TT-seq library construction (see the Supplemental Material). Libraries were pooled and sequenced paired-end with the 200 cycle kit on a NovaSeq S4 single lane.

ChIP-seq sample preparation and library construction

Two days before the time course, cells were plated 1:4 into three 15 cm dishes per sample in SC2 media with 1 μM GSI. Replicates were performed on different days ($n = 2$). Cells were cross-linked with 1% formaldehyde at the indicated time after GSI washout, and chromatin was prepared from the cells (see the Supplemental Material). Thirty microliters of H3K27ac antibody (Active Motive 39133) was used for each IP (see the Supplemental Material). For spike normalization, the same amount of sheared *Drosophila* DNA was added to each sample before library construction. Libraries were prepared using the NEBNext Ultra II DNA library preparation kit for Illumina (New England Biolabs E7645) and sequenced paired-end on a NovaSeq with an S1 single-lane 100 cycle kit.

ATAC-seq sample preparation and library construction

The evening before the time course, cells were plated in 12 well dishes at 125,000 cells/well in SC2 media with 1 μM GSI. Replicates were performed on different days ($n = 2$). At the time point after washout or mock washout, cells were rinsed in PBS, harvested using 0.25% trypsin with GSI and/or BRM014 according to the sample, and quenched with SC2 media containing GSI and/or BRM014. Cells were counted, and 100,000 cells were transferred to an Eppendorf tube and combined with 10,000 fly spike-in cells. The spike-in S2 cells were collected, resuspended in Bambanker cryopreservative media (VWR 101974-112), aliquoted, and stored at −80°C. All spike-in aliquots for one experimental time course replicate were thawed and combined before beginning the time course.

ATAC-seq was performed according to the OmniATAC protocol (see the Supplemental Material; Grandi et al. 2022). Libraries were sequenced paired-end on a NovaSeq with an S1 single-lane 100 cycle kit.

PRO-seq sample preparation

The evening before the time course, cells were plated on nine 10 cm dishes at 5.5 million cells/plate in SC2 media with 1 μM GSI. Replicates were performed on different days ($n = 2$ and $n = 3$ for the reference condition). At the relevant time after washout, plates were rinsed with PBS, and 0.25% trypsin (containing GSI for the mock washout or an equivalent amount of DMSO for all other time points) was added. Once cells were detaching from the plate, trypsin was quenched with cold SC2 media (containing GSI for the mock washout or an equivalent amount of DMSO for all other time points), and cells were transferred to a 15 mL Falcon tube. Cells were permeabilized, and PRO-seq libraries were constructed as described in the Supplemental Material. Pooled libraries were sequenced using the Illumina 200 cycle kit on an S4 single lane, followed by an additional run on a full SP lane for more depth for some samples.

TT-seq mapping

Reads were mapped first to the spike genome (dm6) using bowtie 1.2.2 (Langmead et al. 2009) and then to the human genome (hg38) using STAR2.7.3a (Dobin et al. 2013). See the Supplemental Material for additional mapping parameters. To normalize samples, reads mapping to exons in the active gene models (see below) were counted using featurecounts and used to calculate size factors using DESeq2 (Love et al. 2014). PCA plots were generated using DESeq2 over the top 500 genes. These size factors were scaled so the minimum was 1 and were used to normalize bedGraphs with the custom script normalize_bedGraph.pl. Biological replicates ($n = 2$) were merged using the script bedgraphs2stbedGraph.pl.

ChIP-seq mapping

Reads were mapped first to the spike genome (dm6) and then to the human genome (hg38) using bowtie1.2.2 (Langmead et al. 2009) with options -k1 -v2 – best. The custom script bowtie2stdBedGraph.pl was used to make bedGraph files with a 75 bp shift. As spike returns were not different between time points, samples were depth-normalized using the script normalize_bedGraph.pl. Biological replicates ($n = 2$) were merged using the script bedgraphs2stbedGraph.pl. See the Supplemental Material for additional mapping parameters.

ATAC-seq mapping

Reads were first mapped to the spike genome (dm6), and reads that did not map to the spike were mapped to the human genome (hg38) using bowtie1.2.2 (Langmead et al. 2009). See the Supplemental Material for additional mapping parameters. A custom script, extract_fragments.pl, was used to filter and retain unique reads between 10 and 150 bp, which corresponded to regions of open chromatin, and convert files into bedGraph format. Spike return rates were not significantly different between samples. To normalize samples, reads mapping to the −1 kb to +1 kb region around active promoters in this cell type (see "Genome Annotation" below) were counted using the custom script makeheatmap with the "-b v -v t -s b" options. The number of these reads was used to calculate size factors using DESeq2 (Love et al. 2014). These size factors were scaled so the minimum was 1 and used to normalize bedGraphs with the custom script normalize_bedGraph.pl. PCA plots were generated using DESeq2 over the top 500 promoters. Biological replicates ($n = 2$) were merged using the script bedgraphs2stbedGraph.pl.

PRO-seq mapping

Reads were mapped to a combined genome including both the spike (dm6) and primary (hg38) genomes using bowtie2 (Langmead and Salzberg 2012). See the Supplemental Material for additional mapping parameters. As spike percentages were not significantly different between samples, biological replicates were depth-normalized using the script normalize_bedGraph.pl. PCA plots were generated using DESeq2 using gene body PRO-seq counts over the top 500 genes. Biological replicates ($n = 3$ for $t = 0$, and $n = 2$ for all other time points) were merged using the script bedgraphs2stbedGraph.pl. The merged $t = 0$ bedGraph was normalized by multiplying by 0.66 using normalize_bedGraph.pl so that all time points had an equivalent depth. BedGraph files were binned in 10 bp intervals and converted to bigwig files for visualization on the genome browser using UCSC tools (Kent et al. 2010).

RNA-seq mapping

RNA-seq fastq files from Pan et al. (2020) for samples 4 h after GSI washout (GSM4732270, GSM4732271, and GSM4732272) and after mock washout (GSM4732261, GSM4732262, and GSM4732263) were downloaded from the Sequence Read Archive. Reads were mapped to hg38 using STAR version 2.7.3a (Dobin et al. 2013) as described above in "TT-seq Mapping." Gene counts were determined using the featurecounts function in Rsubread (Liao et al. 2014) package version 2.14.2, and $\log_2$ fold change after 4 h of GSI washout was determined using DESeq2 (Love et al. 2014) version 1.40.2. Samples were normalized using the size factors calculated by DESeq2.

Genome annotation

To select gene-level features for differential expression analysis and for pairing with PRO-seq data, we assigned a single, dominant TSS and transcription end site (TES) to each active gene. This was accomplished using a custom script, get_gene_annotations.sh, which used RNA-seq read abundance and PRO-seq R2 reads (RNA 5′ ends) to identify dominant TSSs and used RNA-seq profiles to define most commonly used TESs. RNA-seq data from Pan et al. (2020) at 0 h (GSM4732261, GSM4732262, and GSM4732263) and 4 h (GSM4732270, GSM4732271, and GSM4732272) after GSI washout were used, and merged PRO-seq data from all conditions in this work were used for this analysis to comprehensively capture gene activity in these samples.

Differential gene expression analysis

TT-seq reads mapping to exons in the active gene models were counted using the featurecounts function in the Rsubread (Liao et al. 2014) package version 2.14.2, and these values were normalized using size factors in DESeq2 (Love et al. 2014) version 1.40.2. Significance values were calculated for each comparison between conditions using the design formula ~replicate + condition. Genes were called significantly changed if they had adjusted P-value < 0.01 and $|FC| > 1.5$ in either the 1h_washout_DMSO or the 4h_washout_DMSO condition versus 0h_GSI_DMSO. Four groups were then assigned: (1) Notch upregulated: significantly upregulated in 1h_washout_DMSO versus 0h_GSI_DMSO and (1h_washout_DMSO/1h_GSI_DMSO) > 1.5 or significantly upregulated in 4h_washout_DMSO versus 0h_GSI_DMSO and (4h_washout_DMSO/4h_GSI_DMSO) > 1.5; (2) Notch downregulated: significantly downregulated in 1h_washout_DMSO versus 0h_GSI_DMSO and (1h_washout_DMSO/1h_GSI_DMSO) < 0.667 or significantly upregulated in 4h_washout_DMSO versus 0h_GSI_DMSO and (4h_washout_DMSO/4h_GSI_DMSO) < 0.667; (3) nonspecific upregulated: significantly upregulated in 1h_washout_DMSO versus 0h_GSI_DMSO and not Notch upregulated; and (4) nonspecific downregulated: significantly upregulated in 1h_washout_DMSO versus 0h_GSI_DMSO and not Notch downregulated. Genes were then filtered to include only those with at least 60 PRO-seq promoter (TSS to TSS + 150 nt) reads in one condition to select only for high-confidence genes. For display in heat maps, experimental replicates were averaged, and gene expression was normalized such that the highest condition being displayed was set to 1.

A list of unchanged genes was defined as genes not significant in any of the above four categories that additionally had a |FC| < 1.10 in either the 1h_washout_DMSO or the 4h_washout_DMSO condition versus 0h_GSI_DMSO ($n = 1484$).

A list of inactive genes was defined as genes with <10 PRO-seq reads within the promoter (TSS to TSS + 150 nt) at any time point ($n = 1295$).

Enhancer identification

PRO-seq single-nucleotide bedgraph files were merged over all time points and converted into bigwig files. dREG (Danko et al. 2015) was used to predict putative regulatory elements using these input files. These were refined using a custom filtering script, dRIP-filter, to keep only peaks with a dREG score of at least 0.5, a *P*-value of <0.025, and at least five PRO-seq reads in two conditions. As an additional validation of enhancer quality, H3K27ac ChIP signal (merged over all time points) was counted over the potential dREG peaks using makeheatmap using the "-b v -v t -s b" options, and only peaks with at least 300 reads were kept. Next, promoter-proximal peaks (within 1 kb of active annotated promoters) were removed, leaving only distal enhancers and enhancers within 1 kb of each other were merged into one window using bedtools merge. Enhancers overlapping rRNAs, snRNAs, scRNAs, srpRNAs, tRNAs, or snoRNAs were removed using bedtools intersect. Enhancers were then classified as intragenic if they overlapped an active gene or intergenic if they did not. Intragenic enhancers overlapping two genes on opposite strands were discarded, leaving a final list of 12,040 intergenic and 8983 intragenic enhancers.

Notch transcription complex (NTC) binding analysis

Eight-thousand-five-hundred-thirty-three ChIP peaks bound by both RBPJ and MAML1, as determined by Pan et al. (2020), were defined as NTC binding regions. The intersectBed tool was used to identify genes with promoter NTC binding—those with an NTC binding region overlapping the 1 kb upstream of the TSS. To identify NTC-bound enhancers, intersectBed was used to label enhancers that overlap an NTC binding region. The distance from a gene TSS to the closest enhancer was calculated using the bedtools closest function.

Assigning enhancers to genes

The closest NTC-bound enhancer (see above) to the TSS of each Notch-upregulated gene was identified using the bedtools closest function. Three genes had no NTC-bound enhancers within 1,000,000 bp of the TSS and were excluded from further analysis, yielding a group of 58 closest enhancers to Notch-upregulated genes, shown in Figure 2, G and H. For aggregate plots shown in Figure 2, E and F, the dominant enhancer TSS for each of these 58 enhancers was identified in order to center the plots. Unannotated TSSs called by TSS-call as part of the genome annotation pipeline (see above) within the dREG peaks were identified using bedtools intersect, and the enhancer with the highest TSS score (from TSS-call) for each enhancer was selected as the dominant enhancer TSS (eTSS). For intragenic enhancers, only eTSSs on the nongene strand were considered. This resulted in a list of 56 enhancers with a dominant eTSS, which are plotted in Figure 2, E and F. A control set of non-NTC-bound enhancers was determined by first choosing the closest enhancer within 1,000,000 bp of unchanged genes from the TT-seq experiment. Bedtools intersect -v was used to remove any enhancers that overlapped an NTC ChIP peak, leaving a set of 932 enhancers (shown in Supplemental Fig. S2B).

Gene ontology enrichment

Biological process GO term enrichment was determined using the Molecular Signatures Database (MSigDB) (Liberzon et al. 2011) website (https://www.gsea-msigdb.org) on all genes in groups 1 and 2. For groups 3 and 4, which had >500 genes, the top 500 genes with the largest (group 3) or smallest (group 4) fold change at 4 h were used as the input.

Summing reads over genomic features

For analysis of PRO-seq reads over genes, genomic windows were defined starting from the active gene annotation. Gene body regions were defined as TSS + 250 nt to TSS + 5 kb or the first intragenic enhancer, whichever came first. Principal component analysis shown in Supplemental Figure S2A was performed over these regions for genes >1 kb in length. TSS windows were defined as TSS to TSS + 150 nt. Reads were counted over these regions using the custom script makeheatmap using the "-b v -l s -s s" options. Counts were normalized by the length of the genomic window.

Total ATAC-seq reads at promoters were counted using makeheatmap using the "-b v -v t -s b" options over a window beginning 450 bp upstream of the TSS to 149 nt downstream from the TSS. This window was chosen to focus on the nucleosome-depleted region at the promoter.

H3K27ac ChIP-seq and ATAC-seq reads over dREG peaks for Figure 3, G and H, were counted using makeheatmap using the "-b v -v t -s b" options on single-nucleotide bedgraph files merged over replicates. The full dREG peak region was chosen for this analysis.

Aggregate plots

For PRO-seq aggregate plots around promoters, PRO-seq reads were counted in 20 nt bins from TSS − 100 nt to TSS + 1 kb, summing the total reads within the window for each gene using makeheatmap with the "-b c -a s -l s -v t -s s" options. For aggregate plots in the gene body, PRO-seq reads were counted in 40 nt bins from TSS + 500 nt to TSS + 1 kb, summing the total reads within the window for each gene. The average value over the Notch upregulated genes for each bin is shown in the plots.

For ATAC-seq aggregate plots at promoters, ATAC-seq reads were counted in 75 bp bins within 1 kb of the gene TSS using makeheatmap with the "-b c -a u -v t -s b" options.

For ATAC-seq and ChIP-seq aggregate plots over dREG peaks, reads were counted around the dominant TSS for the enhancer using makeheatmap with the "-b c -a u -v t -s b" options. ATAC-seq reads were counted in 75 bp bins, and ChIP-seq reads were counted in 50 bp bins.

Calculating pausing indices

Pausing index is defined as PRO-seq reads per base pair in the TSS (TSS to TSS + 150 nt) divided by PRO-seq reads per base pair in TSS + 250 nt to TSS + 2250 nt or TES, whichever came first. Reads in these regions were counted using makeheatmap using the "-b v -l s -s s" options.

Data and code availability

TT-seq, PRO-seq, H3K27ac ChIP-seq, and ATAC-seq data sets have been deposited in GEO (GSE269128) and are publicly available upon publication. Custom scripts have been deposited in Zenodo and are publicly available at https://zenodo.org/records/11222086 and https://zenodo.org/records/6654472. Any additional information required to reanalyze the data reported here is available from the corresponding author on request.

Competing interest statement

S.C.B. is on the board of directors of the nonprofit Institute for Protein Innovation and the Revson Foundation; is on the scientific advisory board for and receives funding from Erasca, Inc., for an unrelated project; is an advisor to MPM Capital; and is a consultant for IFM, Scorpion Therapeutics, Odyssey Therapeutics, Droia Ventures, and Ayala Pharmaceuticals for unrelated projects. J.C.A. is a consultant for Ayala Pharmaceuticals; Cellestia, Inc.; SpringWorks Therapeutics; and Remix Therapeutics. K.A. is a consultant to Syros Pharmaceuticals and Odyssey Therapeutics, is on the Scientific Advisory Board of CAMP4 Therapeutics, and received research funding from Novartis not related to this work. The other authors declare no competing interests.

Acknowledgments

We thank Marie Bao and members of the Blacklow and Adelman laboratories for helpful discussion. We thank the Nascent Transcriptomics Core at Harvard Medical School for performing PRO-seq and TT-seq library construction, and Apoorva Baluapuri, the Harvard Medical School Biopolymers Facility, and the Bauer Core Facility at Harvard University for sequencing.

This work was supported by National Institutes of Health awards R35 CA220340 and R01 CA272484 to S.C.B., and R01GM139960 to K.A.; a National Science Foundation Graduate Research Fellowship (DGE1745303) and the Sophia H.Y Chang Fellowship to C.A.M.; a Canadian Institutes of Health Research Banting Postdoctoral Fellowship to B.J.E.M.; and a Leukemia and Lymphoma Society Career Development Fellowship and K99GM144750 grant to J.M.R.

Author contributions: S.C.B., K.A., J.M.R., and J.C.A. conceived the study and performed the methodology. J.M.R. performed the investigation and curated and visualized the data. J.M.R., C.A.M., and B.J.E.M. analyzed the data. A.P.M. acquired the resources. J.M.R., S.C.B., and K.A. wrote the manuscript. K.A. and S.C.B. supervised the study. J.M.R. and S.C.B. acquired the funding.

References

Adelman K, Lis JT. 2012. Promoter-proximal pausing of RNA polymerase II: emerging roles in metazoans. *Nat Rev Genet* **13:** 720–731. doi:10.1038/nrg3293

Adelman K, Kennedy MA, Nechaev S, Gilchrist DA, Muse GW, Chinenov Y, Rogatsky I. 2009. Immediate mediators of the inflammatory response are poised for gene activation through RNA polymerase II stalling. *Proc Natl Acad Sci* **106:** 18207–18212. doi:10.1073/pnas.0910177106

Aster JC. 2020. Notch signaling in context: basic and translational implications. *Trans Am Clin Climatol Assoc* **131:** 147–156.

Aster JC, Pear WS, Blacklow SC. 2017. The varied roles of Notch in cancer. *Ann Rev Pathol* **12:** 245–275. doi:10.1146/annurev-pathol-052016-100127

Biddie SC, John S, Sabo PJ, Thurman RE, Johnson TA, Schiltz RL, Miranda TB, Sung MH, Trump S, Lightman SL, et al. 2011. Transcription factor AP1 potentiates chromatin accessibility and glucocorticoid receptor binding. *Mol Cell* **43:** 145–155. doi:10.1016/j.molcel.2011.06.016

Boettiger AN, Levine M. 2009. Synchronous and stochastic patterns of gene activation in the *Drosophila* embryo. *Science* **325:** 471–473. doi:10.1126/science.1173976

Bray SJ, Gomez-Lamarca M. 2018. Notch after cleavage. *Curr Opin Cell Biol* **51:** 103–109. doi:10.1016/j.ceb.2017.12.008

Buenrostro JD, Giresi PG, Zaba LC, Chang HY, Greenleaf WJ. 2013. Transposition of native chromatin for fast and sensitive epigenomic profiling of open chromatin, DNA-binding proteins and nucleosome position. *Nat Methods* **10:** 1213–1218. doi:10.1038/nmeth.2688

Castel D, Mourikis P, Bartels SJJ, Brinkman AB, Tajbakhsh S, Stunnenberg HG. 2013. Dynamic binding of RBPJ is determined by Notch signaling status. *Genes Dev* **27:** 1059–1071. doi:10.1101/gad.211912.112

Chambers C, Cermakova K, Chan YS, Kurtz K, Wohlan K, Lewis AH, Wang C, Pham A, Dejmek M, Sala M, et al. 2023. SWI/SNF blockade disrupts PU.1-directed enhancer programs in normal hematopoietic cells and acute myeloid leukemia. *Cancer Res* **83:** 983–996. doi:10.1158/0008-5472.CAN-22-2129

Core L, Adelman K. 2019. Promoter-proximal pausing of RNA polymerase II: a nexus of gene regulation. *Genes Dev* **33:** 960–982. doi:10.1101/gad.325142.119

Danko CG, Hyland SL, Core LJ, Martins AL, Waters CT, Lee HW, Cheung VG, Kraus WL, Lis JT, Siepel A. 2015. Identification of active transcriptional regulatory elements from GRO-seq data. *Nat Methods* **12:** 433–438. doi:10.1038/nmeth.3329

Dobin A, Davis CA, Schlesinger F, Drenkow J, Zaleski C, Jha S, Batut P, Chaisson M, Gingeras TR. 2013. STAR: ultrafast

universal RNA-seq aligner. *Bioinformatics* **29:** 15–21. doi:10.1093/bioinformatics/bts635

Falo-Sanjuan J, Lammers NC, Garcia HG, Bray SJ. 2019. Enhancer priming enables fast and sustained transcriptional responses to Notch signaling. *Dev Cell* **50:** 411–425.e8. doi:10.1016/j.devcel.2019.07.002

Fryer CJ, Lamar E, Turbachova I, Kintner C, Jones KA. 2002. Mastermind mediates chromatin-specific transcription and turnover of the Notch enhancer complex. *Genes Dev* **16:** 1397–1411. doi:10.1101/gad.991602

Gilchrist DA, Dos Santos G, Fargo DC, Xie B, Gao Y, Li L, Adelman K. 2010. Pausing of RNA polymerase II disrupts DNA-specified nucleosome organization to enable precise gene regulation. *Cell* **143:** 540–551. doi:10.1016/j.cell.2010.10.004

Gomez-Lamarca MJ, Falo-Sanjuan J, Stojnic R, Abdul Rehman S, Muresan L, Jones ML, Pillidge Z, Cerda-Moya G, Yuan Z, Baloul S, et al. 2018. Activation of the Notch signaling pathway in vivo elicits changes in CSL nuclear dynamics. *Dev Cell* **44:** 611–623.e7. doi:10.1016/j.devcel.2018.01.020

Grandi FC, Modi H, Kampman L, Corces MR. 2022. Chromatin accessibility profiling by ATAC-seq. *Nat Protoc* **17:** 1518–1552. doi:10.1038/s41596-022-00692-9

Hargreaves DC, Horng T, Medzhitov R. 2009. Control of inducible gene expression by signal-dependent transcriptional elongation. *Cell* **138:** 129–145. doi:10.1016/j.cell.2009.05.047

Heinz S, Benner C, Spann N, Bertolino E, Lin YC, Laslo P, Cheng JX, Murre C, Singh H, Glass CK. 2010. Simple combinations of lineage-determining transcription factors prime *cis*-regulatory elements required for macrophage and B cell identities. *Mol Cell* **38:** 576–589. doi:10.1016/j.molcel.2010.05.004

Hirata H, Yoshiura S, Ohtsuka T, Bessho Y, Harada T, Yoshikawa K, Kageyama R. 2002. Oscillatory expression of the bHLH factor Hes1 regulated by a negative feedback loop. *Science (1979)* **298:** 840–843. doi:10.1126/science.1074560

Iurlaro M, Stadler MB, Masoni F, Jagani Z, Galli GG, Schübeler D. 2021. Mammalian SWI/SNF continuously restores local accessibility to chromatin. *Nat Genet* **53:** 279–287. doi:10.1038/s41588-020-00768-w

Kadam S, Emerson BM. 2003. Transcriptional specificity of human SWI/SNF BRG1 and BRM chromatin remodeling complexes. *Mol Cell* **11:** 377–389. doi:10.1016/S1097-2765(03)00034-0

Kent WJ, Zweig AS, Barber G, Hinrichs AS, Karolchik D. 2010. Bigwig and BigBed: enabling browsing of large distributed datasets. *Bioinformatics* **26:** 2204–2207. doi:10.1093/bioinformatics/btq351

Krejčí A, Bray S. 2007. Notch activation stimulates transient and selective binding of Su(H)/CSL to target enhancers. *Genes Dev* **21:** 1322–1327. doi:10.1101/gad.424607

Kwak H, Fuda NJ, Core LJ, Lis JT. 2013. Precise maps of RNA polymerase reveal how promoters direct initiation and pausing. *Science* **339:** 950–953. doi:10.1126/science.1229386

Lagha M, Bothma JP, Esposito E, Ng S, Stefanik L, Tsui C, Johnston J, Chen K, Gilmour DS, Zeitlinger J, et al. 2013. Paused Pol II coordinates tissue morphogenesis in the *Drosophila* embryo. *Cell* **153:** 976–987. doi:10.1016/j.cell.2013.04.045

Langmead B, Salzberg SL. 2012. Fast gapped-read alignment with bowtie 2. *Nat Methods* **9:** 357–359. doi:10.1038/nmeth.1923

Langmead B, Trapnell C, Pop M, Salzberg SL. 2009. Ultrafast and memory-efficient alignment of short DNA sequences to the human genome. *Genome Biol* **10:** R25. doi:10.1186/gb-2009-10-3-r25

Lefterova MI, Steger DJ, Zhuo D, Qatanani M, Mullican SE, Tuteja G, Manduchi E, Grant GR, Lazar MA. 2010. Cell-specific determinants of peroxisome proliferator-activated receptor γ function in adipocytes and macrophages. *Mol Cell Biol* **30:** 2078–2089. doi:10.1128/MCB.01651-09

Liao Y, Smyth GK, Shi W. 2014. Featurecounts: an efficient general purpose program for assigning sequence reads to genomic features. *Bioinformatics* **30:** 923–930. doi:10.1093/bioinformatics/btt656

Liberzon A, Subramanian A, Pinchback R, Thorvaldsdóttir H, Tamayo P, Mesirov JP. 2011. Molecular Signatures Database (MSigDB) 3.0. *Bioinformatics* **27:** 1739–1740. doi:10.1093/bioinformatics/btr260

Liu K, Shen D, Shen J, Gao SM, Li B, Wong C, Feng W, Song Y. 2017. The super elongation complex drives neural stem cell fate commitment. *Dev Cell* **40:** 537–551.e6. doi:10.1016/j.devcel.2017.02.022

Love MI, Huber W, Anders S. 2014. Moderated estimation of fold change and dispersion for RNA-seq data with DESeq2. *Genome Biol* **15:** 550. doi:10.1186/s13059-014-0550-8

Mahat DB, Kwak H, Booth GT, Jonkers IH, Danko CG, Patel RK, Waters CT, Munson K, Core LJ, Lis JT. 2016. Base-pair-resolution genome-wide mapping of active RNA polymerases using precision nuclear run-on (PRO-seq). *Nat Protoc* **11:** 1455–1476. doi:10.1038/nprot.2016.086

Martin AP, Bradshaw GA, Eisert RJ, Egan ED, Tveriakhina L, Rogers JM, Dates AN, Scanavachi G, Aster JC, Kirchhausen T, et al. 2023a. A spatiotemporal Notch interaction map from plasma membrane to nucleus. *Sci Signal* **16:** eadg6474. doi:10.1126/scisignal.adg6474

Martin BJE, Ablondi EF, Goglia C, Mimoso CA, Espinel-Cabrera PR, Adelman K. 2023b. Global identification of SWI/SNF targets reveals compensation by EP400. *Cell* **186:** 5290–5307.e26. doi:10.1016/j.cell.2023.10.006

Pan L, Lemieux ME, Thomas T, Rogers JM, Lipper CH, Lee W, Johnson C, Sholl LM, South AP, Marto JA, et al. 2020. IER5, a DNA damage response gene, is required for notch-mediated induction of squamous cell differentiation. *eLife* **9:** e58081. doi:10.7554/eLife.58081

Papillon JPN, Nakajima K, Adair CD, Hempel J, Jouk AO, Karki RG, Mathieu S, Möbitz H, Ntaganda R, Smith T, et al. 2018. Discovery of orally active inhibitors of Brahma homolog (BRM)/SMARCA2 ATPase activity for the treatment of Brahma related gene 1 (BRG1)/SMARCA4-mutant cancers. *J Med Chem* **61:** 10155–10172. doi:10.1021/acs.jmedchem.8b01318

Pillidge Z, Bray SJ. 2019. SWI/SNF chromatin remodeling controls notch-responsive enhancer accessibility. *EMBO Rep* **20:** 1–16. doi:10.15252/embr.201846944

Rogers JM, Guo B, Egan ED, Aster JC, Adelman K, Blacklow SC. 2020. MAML1-dependent notch-responsive genes exhibit differing cofactor requirements for transcriptional activation. *Mol Cell Biol* **40:** 1–11. doi:10.1128/MCB.00014-20

Saccani S, Pantano S, Natoli G. 2001. Two waves of nuclear factor κB recruitment to target promoters. *J Exp Med* **193:** 1351–1360. doi:10.1084/jem.193.12.1351

Saint Just Ribeiro M, Hansson ML, Wallberg AE. 2007. A proline repeat domain in the Notch co-activator MAML1 is important for the p300-mediated acetylation of MAML1. *Biochem J* **404:** 289–298. doi:10.1042/BJ20061900

Schick S, Grosche S, Kohl KE, Drpic D, Jaeger MG, Marella NC, Imrichova H, Lin JMG, Hofstätter G, Schuster M, et al. 2021. Acute BAF perturbation causes immediate changes in chromatin accessibility. *Nat Genet* **53:** 269–278. doi:10.1038/s41588-021-00777-3

Schwalb B, Michel M, Zacher B, Frühauf K, Demel C, Tresch A, Gagneur J, Cramer P. 2016. TT-seq maps the human transient

transcriptome. *Science* **352:** 1225–1228. doi:10.1126/science.aad9841

Siebel C, Lendahl U. 2017. Notch signaling in development, tissue homeostasis, and disease. *Physiol Rev* **97:** 1235–1294. doi:10.1152/physrev.00005.2017

Skalska L, Stojnic R, Li J, Fischer B, Cerda-Moya G, Sakai H, Tajbakhsh S, Russell S, Adryan B, Bray SJ. 2015. Chromatin signatures at Notch-regulated enhancers reveal large-scale changes in H3K56ac upon activation. *EMBO J* **34:** 1889–1904. doi:10.15252/embj.201489923

Takeuchi JK, Lickert H, Bisgrove BW, Sun X, Yamamoto M, Chawengsaksophak K, Hamada H, Yost HJ, Rossant J, Bruneau BG. 2007. Baf60c is a nuclear Notch signaling component required for the establishment of left–right asymmetry. *Proc Natl Acad Sci* **104:** 846–851. doi:10.1073/pnas.0608118104

Utley RT, Côté J, Owen-Hughes T, Workman JL. 1997. SWI/SNF stimulates the formation of disparate activator-nucleosome complexes but is partially redundant with cooperative binding. *J Biol Chem* **272:** 12642–12649. doi:10.1074/jbc.272.19.12642

van den Ameele J, Cheetham SW, Krautz R, Donovan APA, Llorà-Batlle O, Yakob R, Brand AH. 2022. Reduced chromatin accessibility correlates with resistance to Notch activation. *Nat Commun* **13:** 2210. doi:10.1038/s41467-022-29834-z

Wang H, Zou J, Zhao B, Johannsen E, Ashworth T, Wong H, Pear WS, Schug J, Blacklow SC, Arnett KL, et al. 2011. Genome-wide analysis reveals conserved and divergent features of Notch1/RBPJ binding in human and murine T-lymphoblastic leukemia cells. *Proc Natl Acad Sci* **108:** 14908–14913. doi:10.1073/pnas.1109023108

Wang H, Zang C, Taing L, Arnett KL, Wong YJ, Pear WS, Blacklow SC, Liu XS, Aster JC. 2014. NOTCH1–RBPJ complexes drive target gene expression through dynamic interactions with superenhancers. *Proc Natl Acad Sci* **111:** 705–710. doi:10.1073/pnas.1315023111

Weinmann AS, Mitchell DM, Sanjabi S, Bradley MN, Hoffmann A, Liou H-C, Smale ST. 2001. Nucleosome remodeling at the IL-12 p40 promoter is a TLR-dependent, Rel-independent event. *Nat Immunol* **2:** 51–57. doi:10.1038/83168

Weng AP, Millholland JM, Yashiro-Ohtani Y, Arcangeli ML, Lau A, Wai C, Del Bianco C, Rodriguez CG, Sai H, Tobias J, et al. 2006. *c-Myc* is an important direct target of Notch1 in T-cell acute lymphoblastic leukemia/lymphoma. *Genes Dev* **20:** 2096–2109. doi:10.1101/gad.1450406

Yatim A, Benne C, Sobhian B, Laurent-Chabalier S, Deas O, Judde JG, Lelievre JD, Levy Y, Benkirane M. 2012. NOTCH1 nuclear interactome reveals key regulators of its transcriptional activity and oncogenic function. *Mol Cell* **48:** 445–458. doi:10.1016/j.molcel.2012.08.022

Notch induces transcription by stimulating release of paused RNA polymerase II

Julia M. Rogers, Claudia A. Mimoso, Benjamin J.E. Martin, et al.

Genes Dev. published online October 16, 2024
Access the most recent version at doi:10.1101/gad.352108.124